Stochasticity in Single-Molecule Nanoelectrochemistry: Origins, Consequences, and Solutions

Pradyumna S. Singh,[†] Enno Kätelhön,[‡,§] Klaus Mathwig,[†] Bernhard Wolfrum,[‡,§] and Serge G. Lemay[†,*]

[†]MESA+ Institute for Nanotechnology, University of Twente, 7500 AE Enschede, The Netherlands and [‡]Institute of Bioelectronics (ICS-8/PGI-8) and [§]JARA-Fundamentals of Future Information Technology, Forschungszentrum Jülich GmbH, 52425 Jülich, Germany

ABSTRACT Electrochemical detection of single molecules is being actively pursued as an enabler of new fundamental experiments and sensitive analytical capabilities. Most attempts to date have relied on redox cycling in a nanogap, which consists of two parallel electrodes separated by a nanoscale distance. While these initial experiments have demonstrated single-molecule detection at the proof-of-concept level, several fundamental obstacles need to be overcome to transform the technique into a realistic detection tool suitable for use in more complex settings (*e.g.*, studying enzyme dynamics at single catalytic event level, probing neuronal exocytosis, *etc.*). In particular, it has become clearer that stochasticity—the hallmark of most single-molecule measurements—can become the key limiting factor on the quality of the information that can be obtained from single-molecule electrochemical assays. Here we employ random-walk simulations to show that this stochasticity is a universal feature of all single-molecule experiments in the diffusively coupled regime and emerges due to the inherent properties of Brownian motion. We further investigate the intrinsic coupling between stochasticity and detection capability, paying particular attention to the role of the geometry of the detection device and the finite time resolution of measurement systems. We suggest concrete, realizable experimental modifications and approaches to mitigate these limitations. Overall, our theoretical analyses offer a roadmap for optimizing single-molecule electrochemical experiments, which is not only desirable but also indispensable for their wider employment as experimental tools for electrochemical research and as realistic sensing or detection systems.

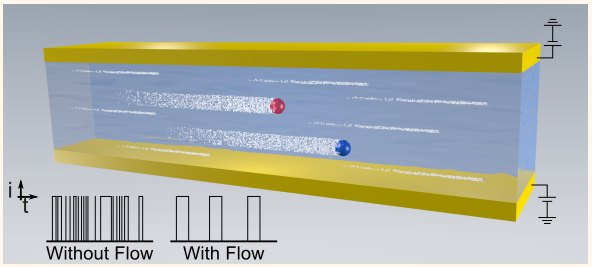

KEYWORDS: nanoelectrochemistry · single-molecule electrochemistry · redox cycling · nanofluidics · nanochannel · stochastic electrochemistry · random walks

The advent of techniques for detecting and manipulating individual molecules in solution counts among the most impactful developments of the last two decades.[1] Currently, the most mature and established single-molecule techniques rely on either force transduction[2] or optical methods.[3] For example, a particularly powerful approach is fluorescence: the detection of single fluorophores[4,5]—even within living cells[6−8]—has become a widespread tool in many branches of science. Similarly sensitive probes based on purely electrical or electrochemical detection, whether through electrostatic coupling or *via* the transfer of electrons between the molecule and an electrode, are being actively pursued, both as enablers of new types of fundamental experiments and as sensor elements in integrated lab-on-a-chip devices.

The main strategy for detecting single molecules *electrochemically* is so-called redox cycling,[9,10] the repeated oxidation and reduction of a target analyte, which allows each molecule to contribute multiple electrons to the overall current. Such an approach was used by Fan and Bard[11−13] in a scanning electrochemical microscope (SECM) configuration: nanometer-high cavities were formed by impinging a wax-coated metal tip onto a conducting substrate. A related approach was employed by Sun and Mirkin by immersing recessed nanoelectrodes in a mercury drop.[14] Most recently, our group demonstrated single-molecule sensitivity in microfabricated nanoelectrochemical devices, which consist of twin electrodes embedded in a nanochannel with interelectrode spacings of 70 nm.[15] Current fluctuations with amplitudes of 20 fA were shown to be consistent with the entry and egress of single individual molecules through the detection volume of the device. Single nanoparticles functionalized by redox-active moieties[16] can also, in principle, be detected using the same strategy.[17]

* Address correspondence to s.g.lemay@utwente.nl.

Received for review July 11, 2012 and accepted October 27, 2012.

Published online October 28, 2012
10.1021/nn3031029

Can these experiments progress from (initially important) one-off proof-of-concept demonstrations to robust, reliable, and routine detection tools in more complex experiments? We believe that the use of microfabrication methods for the development of nanogap transducers embedded in fluidic nanochannels offers a viable route due to several advantages over traditional tip-based methods: devices with identical geometries within a high degree of precision can be fashioned,[18] a variety of geometries can be generated which can be tailored to the intended application,[19] and integration with microfluidic systems is facilitated. Consequently, the approach is scalable to more complex experiments under a diverse set of conditions. Nonetheless, significant conceptual and experimental hurdles remain to be overcome. Most importantly on the conceptual side, most realistic experimental situations require coupling of the nanoscale detection region to some type of reservoir from which a sample containing the analyte of interest is introduced. This however allows single molecules undergoing Brownian motion to enter and leave the detection region at random, creating an inherently stochastic response. That is, the system is nondeterministic and its description is necessarily probabilistic. This was manifest in single-molecule efforts reported thus far, whether *via* inadvertent cracks in the wax insulation around a tip[11] or the presence of a purpose-made access channel[15] (a notable exception being the experiments of Sun and Mirkin[14]). This particular kind of stochasticity in single-molecule signals raises important questions about the widespread applicability of this approach as a probe in "real" analytical systems, where usually sensitive, accurate measurements are required to be carried out in rapid time in a reproducible and deterministic manner.

Here, we explore the fundamental limitations of redox-cycling-based electrochemical detection of single molecules using random-walk simulations.[20−23] These simulations capture the essential behavior of freely diffusing molecules in solution and reveal that, while most experimental approaches to date have focused on enhancing the current per molecule by reducing the interelectrode separation, the free diffusion of molecules imposes its own inherent limitation on the quality of information that can be derived in such experiments, even with an "ideal" measurement system. We further investigate the influence of various factors such as the geometry of the detection region, the mechanism of coupling to the bulk reservoir, and the effect of finite time resolution of the measurement electronics. We conclude by discussing possible experimental alternatives to overcome the limitations imposed by the stochastic nature of Brownian motion, with a view to enable more widespread deployment of this detection strategy in sensitive analytical systems or complex fundamental experiments.

The paper is organized as follows: We first discuss a three-dimensional (3D) diffusion model of a molecule undergoing redox cycling between two electrodes. We then show that the behavior on the time scales of interest can equally be well-described by a much simpler one-dimensional (1D) model that captures the behavior of molecules diffusing in and out of a detection region. We then assess the role of the finite bandwidth of the measurement electronics since, coupled with the stochastic nature of Brownian motion, these two factors impose the most important limitation upon the quality of information one can obtain in a single-molecule experiment. Finally, we discuss ways to overcome these limitations either by trapping the molecule or through the implementation of directed flow (advection) in the system.

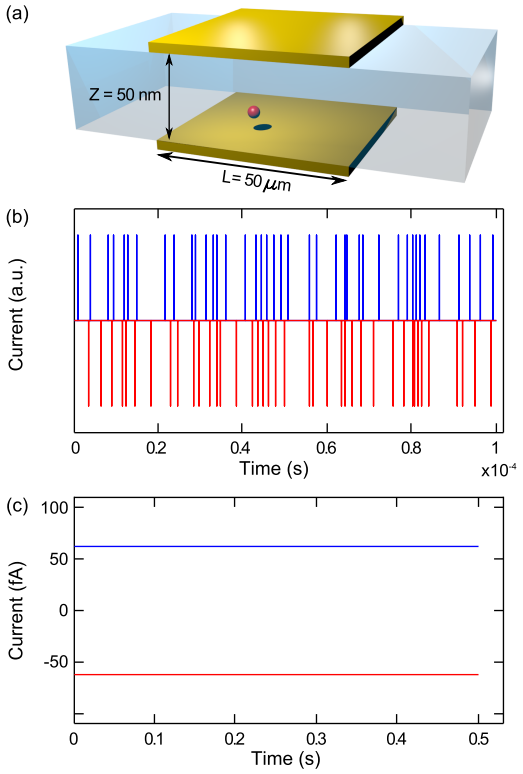

Figure 1. (a) Schematic geometry of a prototypical device invoked for the simulations. (b) Individual electron-transfer events corresponding to oxidation (blue) and reduction (red) of a redox-active molecule confined within the detection region of the device. The area enclosed by each spike corresponds to the charge on one electron, $-e$. (c) Oxidation and reduction currents obtained after averaging and convolving the currents in (b) with an instrumental impulse response with a time constant of 100 ms.

THEORY

In order to facilitate interpretation and relevant comparison with experiments, the ensuing discussion will invoke a prototypical detection device with realistic geometric and experimental parameters, as sketched in Figure 1a. The detection region of this nanogap device is the volume enclosed by the two plane-parallel electrodes constituting the floor and roof of a nanochannel.

The electrodes are separated by a distance z = 50 nm, and the length of the electrodes is L = 50 μm. The detection region is assumed to extend across the whole width of a nanochannel. We further assume that this device is connected to bulk reservoirs *via* nanochannels on both ends through which analyte molecules are introduced in the system. These molecules are free to diffuse in and out of the detection region of the device. The molecules are assigned a diffusion coefficient, $D = 1 \times 10^{-9}$ m^2/s; this value is typical since it lies within the experimentally determined diffusion coefficients of ferrocenyl species in aqueous and non-aqueous solutions. Microfabrication methods allow such geometries to be achieved.[24,25] Recently, SECM configurations have also been demonstrated that achieve spacings on the order of 100 nm.[26] In all of these cases, because the electrode dimensions themselves are much larger than the very small interelectrode separation, the resulting geometry has a very highly skewed aspect ratio ($z \ll L$). As we will argue below, this can be exploited to greatly simplify the theoretical modeling of the system.

When molecules are present in the detection region of the device, they undergo redox cycling, which leads to a current through the electrodes. The behavior of an analyte molecule as it traverses the device can be analyzed at various scales of both length and time, and because of the skewed geometry, these time scales can usually be separated. On the ultrafast time scales, one can, in principle, observe the discreteness of each individual shuttling event as the molecule impinges on one electrode or the other.[27] For the geometry considered here, this time scale would be on the order of $\tau_s \sim z^2/D$ = 2.5 μs. Figure 1b shows current resulting from a full 3D Brownian dynamics simulation of such a particle in the prototypical geometry (for details of the simulation and the geometry used, see Supporting Information). Each spike in Figure 1b corresponds to a single encounter with the electrode and the subsequent transfer of a single electron. Note that the spikes alternate sequentially between the oxidizing and the reducing electrode. This is expected: after an oxidation event, the molecule must of necessity be reduced before it can be oxidized again.

These simulations assumed an extremely high time resolution, Δt = 1 ns. In practice, however, sensitive electrochemical instrumentation systems typically have a measurement bandwidth that is much slower than this time scale in order to achieve sufficient sensitivity. The effect of a (linear) measurement circuit on a time-dependent signal can easily be accounted for by computing the convolution of the "real" signal with the so-called impulse response of the electronics. This convolution is effectively a weighted average of the signal, with the weight being determined by the impulse response. For a simple first-order low-pass filter with a cutoff frequency of $f^0 = 1/2\pi\tau$, the impulse response is simply a decaying exponential, $(1/\tau)\exp(-t/\tau)$, with time constant τ. Figure 1c shows simulated data like those in Figure 1b after convolution with an instrumental time response of τ = 100 ms. The effect is dramatic: the individual electron-transfer events are no longer resolved, and the observed current is instead essentially constant. The magnitude of this current, $i_p \approx$ 64 fA, corresponds to the value expected for one freely diffusing molecule, $i_p = neD/z^2$, where n is the number of electrons transferred per encounter with the electrode and $-e$ is the charge on the electron.[11] Similar arguments regarding the limiting role of the instrument response have been made previously by Amatore *et al.* regarding the observation of individual electron-transfer events in PAMAM dendrimers capped with ruthenium(II) bisterpyridine redox moieties adsorbed on Pt nanoelectrodes.[28]

Consequently, although the molecules undergo diffusion in three dimensions, the dimension perpendicular to the electrodes can be safely ignored since the experimentalist is essentially "blind" to the motion in these directions. Furthermore, in the channel-like geometry assumed here, motion parallel to the electrodes but perpendicular to the axis of the channel is irrelevant since the walls of the channel confine molecules to the channel in this direction. Motion along the axis of the channel, on the other hand, cannot be ignored: the typical time scale for diffusive transport along this dimension is $\tau \sim L^2/D$ = 2.5 s, which is readily accessible in experiments. Therefore, while a comprehensive description of microscopic trajectories must necessarily incorporate diffusion in all dimensions, the use of 2D or 3D simulations adds little in practice for understanding experimentally relevant channel-like nanogap systems since the main observable experimentally is the entry and egress of individual molecules from the detection region of the device. For this reason, we focus below on random-walk simulations in only one dimension, namely, along the length of the detection region. This allows focusing on the features of the system that are most relevant for experiments.

We consider one-dimensional random walks undertaken by a discrete particle. The detection region of the device of length L (μm) is described by a lattice points on which the particle undertakes its random walk. The molecules can move discretely on this lattice with steps of $\pm$1. In real units, the steps therefore have length $\Delta L = L/a$. The corresponding time interval between each step is $\Delta t = (\Delta L)^2/2D$. At each step, the particles can take a unit step to the right with a probability 1/2 or to the left with a probability 1/2. While here we only consider discrete steps of fixed size, one could also, in principle, represent each step with a continuous distribution. However, the probability distribution obtained for the random walk on length scales longer than ΔL is the same in both cases.[29] We therefore use the simpler, discrete model which is more amenable to analytical analysis. The boundaries of the detection region and the presence of the reservoir were simulated

in different ways depending on the purpose of each specific simulation, as described in the Methods section.

RESULTS

Time Evolution. Figure 2 shows a trajectory generated for a single particle as it undergoes a random walk. The shaded gray represents the detection region. At each step, we assess whether the particle is in the detection area of the device or outside it. If it is inside the detection area of the device, we define the occupancy in the device to be 1, else to be 0 (in an experiment, a molecule in the detection region of the device contributes i_p amount of current and 0 current otherwise). As the particle undergoes its random walk, it can repeatedly enter and leave the detection region, leading to rapid telegraph-like oscillations in the current–time response with varying amount of time spent in the detection region for each event, as seen in Figure 2b. Most often, the molecule spends only a very short time in the detection region before exiting again, leading to very rapid oscillations of the occupancy.

Distribution of Residence Times. What is the typical time spent by the particle in the detection region? Our intuition about Brownian motion suggests that this should be on the order of $L^2/2D$. This reasoning is however misleading. The duration of an event is by definition the time elapsed between the moment that a molecule enters the detection region and the moment when it leaves the detection region for the *first* time, a quantity known as the time of first passage. Much is known about first passage times since they are of great interest in diverse fields such as neuroscience, diffusion-controlled chemical reactions, ecology, and finance.[30,31] For the present case, after a particle has entered the device, there is, in principle, an infinite set of trajectories that the particle can follow until it leaves for the first time. The resulting distribution of residence times is given by the solution to the classic Gambler's Ruin problem in random-walk theory.[32] The probability of the particle lasting n steps in the device before it encounters either end of the device for the first time has the analytic form[33]

$$P_{tot}(n) = \frac{1}{a}\left(\sum_{v=1}^{a-1} \cos^{n-1}\frac{\pi v}{a} \sin\frac{\pi v}{a} \sin\frac{\pi v}{a} + \sum_{v=1}^{a-1} \cos^{n-1}\frac{\pi v}{a} \sin\frac{\pi v}{a} \sin\frac{\pi v(a-1)}{a}\right) \quad (1)$$

Here, a is once again the number of lattice points that make up the length of the device, and n can be converted into residence time, t, according to $t = n(\Delta L^2/2D)$. In eq 1, the first term within brackets corresponds to the probability of exiting from the same side that the particle enters, while the second term corresponds to the probability of traversing the detection region and exiting at the other end of the device.

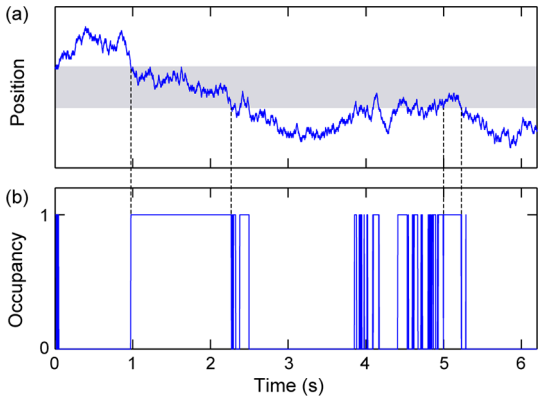

Figure 2. (a) Trajectory of a particle as it undergoes a random walk. The gray region denotes the detection region. (b) Corresponding occupancy plot of the particle within the defined detection region.

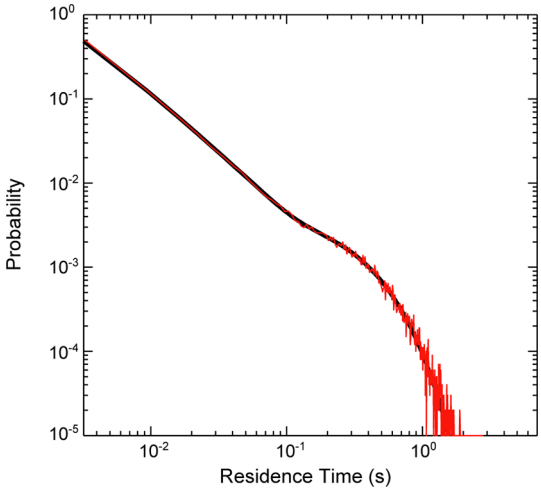

Figure 3. Distribution of residence times of the molecule in the detection region. The black line denotes the distribution calculated according to eq 1, while the red line is the corresponding distribution from a random-walk simulation.

Figure 3 compares the analytically computed probability distribution and the simulated distribution of residence times. There is excellent agreement, naturally, since both simulation and analytical calculation represent the same model. The plot further shows that the most probable residence times are very short. This is a consequence of the fact that it is more likely for the molecule to exit very quickly from the same side as it has entered than to propagate toward the center of the device. At short time scales, the probability distribution diverges as $t^{-3/2}$, where t is the residence time. Thus, even if the motion of the particles was probed on a much faster time scale, the same behavior would be observed. On longer time scales, a "shoulder" is seen in the probability distribution, which corresponds to the alternative scenario where the particle traverses the entire length of the device and exits from the other end. The mean time for first passage, considering only these latter events, is given by $L^2/6D$, consistent with intuition.[15,30]

How does this rapid entry and exit of molecules compare with typical experimental time scales? The inverse relationship between the gain and the measurement bandwidth of amplifiers in electronic measurement circuits ensures that the more sensitive a current measurement system, the lower its time resolution. In particular, the impulse response of electrometers capable of measuring femtoampere level currents is on the order of a few hundred milliseconds.[15] Comparing this to the distribution of residence times (Figure 3), it is clear that most events have residence times that are much shorter than this experimentally accessible time scale, and only the relatively rare, atypically long events can be resolved.

The consequence of finite time resolution is further illustrated in Figure 4a, which shows a typical occupancy–time trace obtained for the case of $\langle N \rangle = 0.2$. As expected, it reveals rapid telegraph-like oscillations corresponding to the presence of 0, 1, or 2 molecules over time. To reproduce the effect of the instrument, this trace was then convolved with a first-order impulse response as described earlier (τ = 100 ms). This filtering results in considerable smoothing of the occupancy–time trace (Figure 4b) such that only the events of durations much longer than τ are able to attain the full magnitude of occupancy as in the unfiltered case. On the other hand, the very rapid events are heavily averaged and not individually resolved in the convolved traces. This leads to noisy-looking curves with apparent plateaus at values of the current that do not correspond to integer number of particles.

It is, in principle, possible to deconvolve the smoothed curve to recover the original data. In practice, this is not possible, however, due to the presence of additional instrumental noise superimposed on the single-molecule signals in experimental data. This noise is amplified by the deconvolution procedure, leading to no improvement in the quality of the signals.

Quantifying the Occupancy. In order to extract quantitative information from stochastic signals, a statistical description is required. The average occupancy in the detection region of the device, $\langle N \rangle$, can be controlled *via* the bulk concentration of the reservoir, C, since the two are in diffusing equilibrium. Neglecting double-layer effects, which is appropriate under the high salt conditions considered here, this is simply $\langle N \rangle = CVN_A$, where N_A is Avogadro's constant and V is the volume of the detection region of the device (more generally, $\langle N \rangle$ is set by the chemical potential of the reservoir). As was made manifest by Figure 4a, however, the instantaneous number of molecules present, $N(t)$, cannot be controlled and stochastic fluctuations between different values of N occur. In general, the probability of having exactly N particles at any given time, P_N, is given by the Gibbs distribution, $P_N \propto Z_N \exp(\mu N/k_BT)$, where Z_N is the partition function for N particles, μ is the chemical potential of the redox species, k_B is Boltzmann's

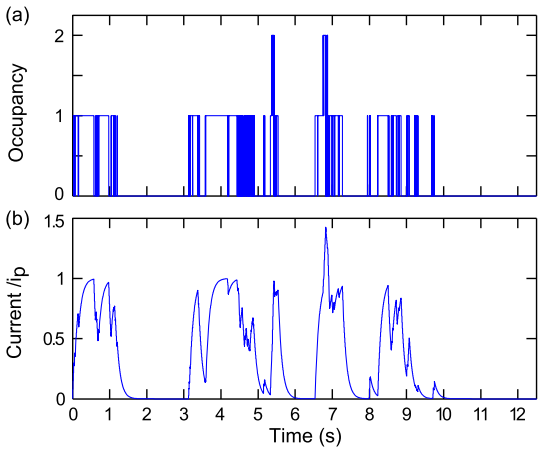

Figure 4. (a) Occupancy–time trace for an average occupancy, $\langle N \rangle = 0.2$. (b) Corresponding current–time plot after convolving the trace in (a) with a model impulse response with a time constant τ = 100 ms. This shows how the finite time response of the measurement electronics precludes the observation of rapid rise and fall in current as the molecule enters and leaves the detection region.

constant, and T is the absolute temperature.[34] For the case of non-interacting particles, which is appropriate for a dilute solution, this is analogous to an ideal gas; in this case, the probability distribution reduces to the well-known Poisson distribution, $P_N = \langle N \rangle^N \exp(-\langle N \rangle)/N!$.[11–13,15]

Figure 5a,d,g shows the probability distributions obtained by histogramming occupancy–time traces generated by random-walk simulations for three different values of $\langle N \rangle$. In order to get sufficient statistics, simulations of 10^5 time steps were repeated 200 times. The resulting probability amplitudes agree to within 1% with the Poisson distribution for P_N.

Implicit in this analysis is the assumption of infinite time resolution. To evaluate the experimentally feasible distribution, we convolved the simulated occupancy–time traces with the assumed impulse response and then histogrammed the resulting traces. Figure 5e,f shows histograms obtained for two different time constants of the impulse response, τ = 0.1 and 1 s, respectively, for $\langle N \rangle = 1$. In comparison to the unfiltered traces, the histograms for the filtered traces are considerably smeared, such that the weight in the probability distribution shifts from the peaks to values intermediate between integer multiples of i_p. This effect becomes more pronounced as τ increases.

The basis of this smearing of histograms can be understood by considering the broad distribution of residence times together with the finite time resolution inherent to measurement systems. Because the vast majority of events are of very short durations, they are heavily smoothed in experiments, resulting in values of current that are much smaller than i_p. The longer events which do result in integer multiples of i_p for the current are rare and make only a minor contribution to the histograms. Taken together, these two factors preempt the observation of distinct peaks in

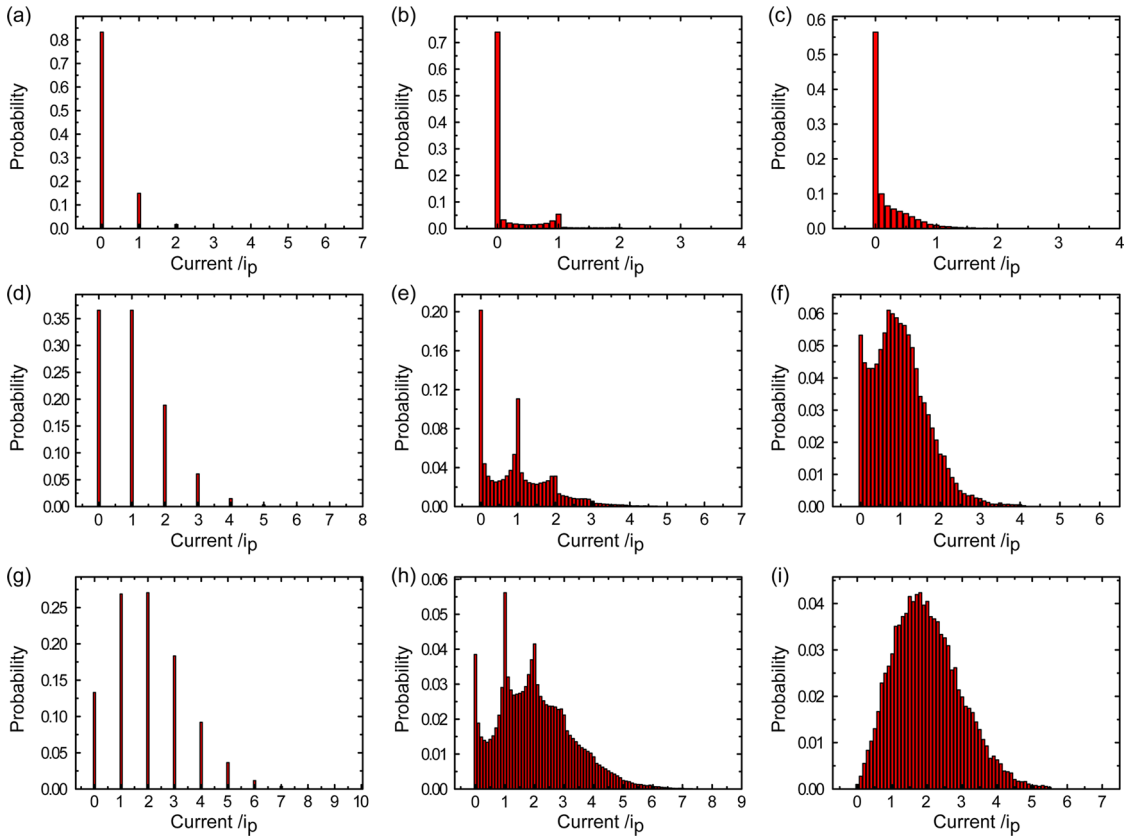

Figure 5. Histograms of simulated traces for different average occupancies and measurement time constants. Rows (top to bottom): Average occupancies of $\langle N \rangle$ = 0.2, 1, and 2, respectively. Columns (left to right): Traces filtered with varying time constants of the impulse response, τ = 0, 0.1, and 1 s, respectively.

the histograms corresponding to the presence of integer number of molecules. We emphasize that this limitation arises from the fundamental properties of Brownian motion of particles since we have not included any extrinsic noise (*e.g.*, instrumental noise) to the traces. Needless to say, the unavoidable presence of extrinsic noise in any measurement will only exacerbate the smearing of histograms.

OVERCOMING STOCHASTICITY

We have seen how the intrinsic properties of random walks combined with the finite time resolution of measurement systems act in concert to limit the ability to resolve single molecules. We now explore possible approaches to mitigate this effect.

Role of Access Channel. In the geometry of the device considered thus far, the detection region is connected to 1D access channels on either side through which molecules can enter. The sharp boundary between the channel and the detection region, coupled with the space-filling property of random walks, increases the likelihood that most trajectories of particles follow a back-and-forth path at the edge. However, what if the detection region of the device was directly connected to a 3D reservoir? One would expect qualitatively different behavior because, unlike in 1D, there is only a small chance in a 3D random walk that the particle will return to its point of origin. In other words, there is high probability that, once a particle diffuses to the edge of the detection region and enters the 3D reservoir, it escapes forever. While not influencing the distribution of dwell times, this should eliminate the clustering of short events and could thus potentially reduce the smearing out of histograms.

Figure 6a shows occupancy–time traces obtained in this way for $\langle N \rangle$ = 0.2. Comparing with Figure 4a shows that, unlike the case of the 1D reservoir where long portions of the trace have 0 occupancy, in the present case, the short events are distributed fairly uniformly. As a result, the long events in the convolved data (Figure 6b) appear less noisy. Comparing the corresponding histogram (Figure 6c) to those of Figure 5, the only difference is that, in the present case, the amplitude corresponding to 0 occupancy is much reduced. However, for the peaks of interest, there is no significant difference between the two cases. We therefore conclude that coupling to a 3D reservoir instead of a 1D channel represents only a minor improvement to the system's ability to resolve single-molecule events.

Trapping of Molecules. We now consider another possible mechanism by which to overcome stochasticity—trapping of molecules in the detection region. While conceptually straightforward, this approach has the

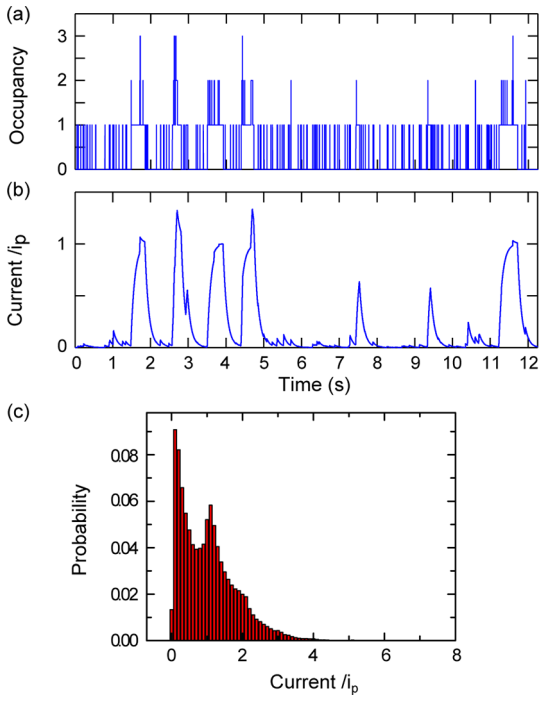

Figure 6. (a) Occupancy−time plot for a device configuration in which the detection region is directly coupled to a 3D reservoir, with an average occupancy of $\langle N \rangle = 0.2$. (b) Corresponding current−time plot after convolving the trace in (a) with a model impulse response with a time constant, $\tau = 100$ ms. (c) Histogram of the convolved traces for an average occupancy of $\langle N \rangle = 1$.

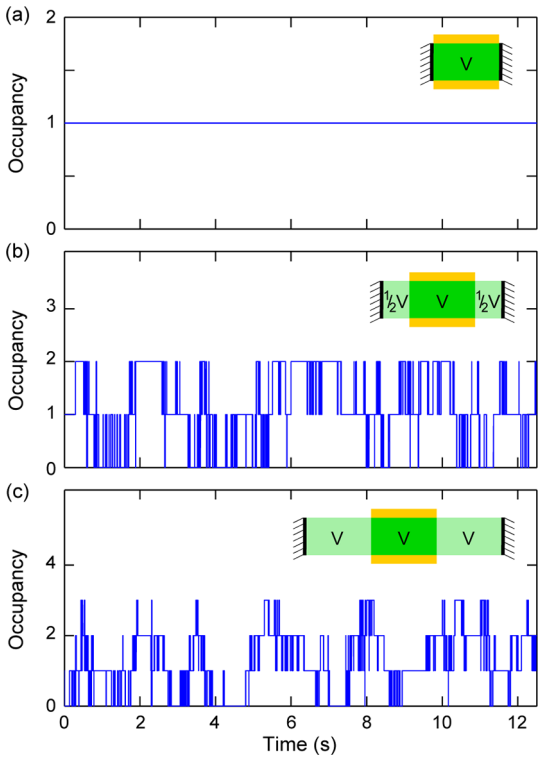

Figure 7. Occupancy traces for particles trapped in the device with sealed boundaries for (a) $V_{dead} = 0$; (b) $V_{dead} = V$; and (c) $V_{dead} = 2V$. The inset in each plot shows the associated geometry. In all cases, the assumed average occupancy in the detection region is $\langle N \rangle = 1$.

disadvantage that a reference electrode can no longer be employed. The earliest examples of electrochemical detection of single molecules adopted this strategy:[11] an electrode that was shrouded by insulating wax was pressed against a conducting substrate, thereby sealing off the detection volume from the external solution. However, fluctuations in the current were still observed which were attributed to intermittent trapping. More recently, Sun and Mirkin were able to ensure trapping of molecules in nanoscale cavities.[14] Although they did not perform amperometric measurements, the number of trapped molecules was inferred from the (essentially time-independent) magnitude of the limiting currents in cyclic voltammetry experiments.

In the context of an integrated nanofluidic system, any analytical method that relies on the mechanical trapping of molecules within the detection region would require some manner of valves[35] to automate the opening and closing of access to the device. Such valves are likely to result in some dead volume on either extremity of the detection region. Here we explore the effect of this dead volume on stochasticity of the resultant current. We assume that the average occupancy in the detection region is $\langle N \rangle = 1$. Further, we define the total volume of the system V_{total} to include the volume of the detection region (V) and the dead volume (V_{dead}). We investigate the effect of keeping $\langle N \rangle$ constant and increasing V_{total}. For the case $V_{dead} = 0$, the occupancy is equal to 1. Thus, amperometrically, only a constant current i_p is expected, as shown in Figure 7a. If, however, there is some dead volume present on either side of the detection region, into which molecules can diffuse, then fluctuations in the occupancy (and current) will be seen. The probability of finding N molecules in the detection region is simply given by the binomial distribution,

$$P_N = \binom{\langle N \rangle / p}{N} p^N (1 - p)^{(\langle N \rangle / p) - N}$$

where $p = V/V_{total}$ is the individual probability of finding each particle in the detection region. Figure 7b shows the occupancy traces obtained for $V_{total} = 2V$. As expected, the occupancy has a binomial distribution, with $P_1 = 0.5$ and $P_0 = P_2 = 0.25$ (see Supporting Information). As the dead volume increases (Figure 7c), however, the occupancy traces become increasingly indistinguishable from the case where there is no trapping and the detection region is coupled to an infinite reservoir (see histograms in Supporting Information). This is not surprising since the binomial distribution asymptotically converges to the Poisson distribution for small p and large N. Experimentally, this implies that, for any improvements from confinement to be noticeable, the dead volume

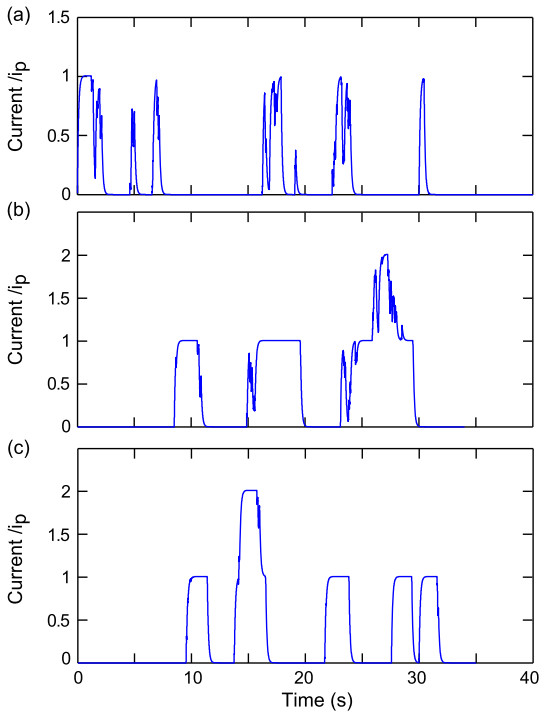

Figure 8. Current−time traces in the presence of flow with different fluid flow velocities in a device with $L = 200\ \mu$m: (a) 1 μm/s, (b) 50 μm/s, (c) 100 μm/s. In all cases, the traces have been convolved with an impulse response with time constant $\tau = 100$ ms.

must be significantly smaller than V. Alternatively, the measurement must integrate over such a long period of time ($\gg L_{total}^2/D$, where L_{total} is the total length including the length along the dead volume) that the fluctuations are averaged over. In this sense, trapping of molecules benefits from small device dimensions.

Hydrodynamic Flow. A way to overcome stochasticity that is particularly suitable for fluidic devices is through the introduction of advective flow in the system. We use the term *advection* to denote a flow that is parallel to the surface of the two electrodes so as to distinguish it from *convection*, which is typically used to describe perpendicular flow. The solution containing the redox-active analyte could be advected through the device using either pressure or electrokinetic methods. This is particularly relevant for cases where sample exchange is desirable. Since advective flow disrupts the diffusive equilibrium between the detection region and the outside, how does it impact the stochasticity of the signals? The main effect is to directly alter the residence time of the molecule in the detection region, with the average residence time given by $t_{flow} = L/v$, where v is the velocity of the fluid and L is the length of the detection region as above. Because the instantaneous rms velocity of the molecules is much larger than v, diffusion (and therefore i_p) remains entirely unaffected; the flow merely introduces a persistent bias. In order for the flow to be effective in creating a well-defined residence time, however, the rms fluctuations in the displacement due to diffusion, Δx, should be much less than the length of the device: $\Delta x = (2D\Delta t_{flow})^{1/2} \ll L$. Rearranging, this leads to a condition for the required velocity, $v \gg 2D/L$. For a device of length $L = 200\ \mu$m, this corresponds to $v \gg 10\ \mu$m/s.

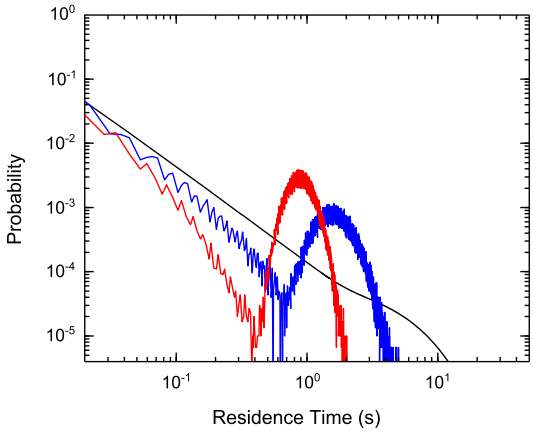

Figure 9. Distribution of residence times as a function of fluid flow velocity obtained from simulations for a device with $L = 200\ \mu$m. Red, 200 μm/s; blue, 100 μm/s; black, analytical solution (in the absence of flow) using eq 1. The small, noise-like oscillations arise from interference between the two discrete step sizes present in the simulation.

Figure 8 shows occupancy traces for three different fluid velocities. For the case where v is less than the critical value (Figure 8a), the occupancy trace shows short events similar to the case where there is no flow in the system. Conversely, when v is much greater than the critical value (Figure 8b,c), the short events are no longer seen, and the occupancy traces show uniform, well-defined residence times in the detection region. Figure 9 shows the simulated distribution of residence times under conditions of fluid flow. A prominent, well-defined peak develops at values of the residence time close to the advection time (near 2 s in Figure 9) that correspond to particles that enter from one side of the device and exit from the other. As can be seen, increasing the fluid velocity shifts this peak to shorter residence times, consistent with intuition. It also increases the absolute probability of such events occurring, especially compared to the case when there is no flow in the system. The simulated curves also show small, very rapid oscillations; these are an artifact of the simulation that arise from having two discrete step sizes of varying lengths corresponding to diffusion and flow (ΔL and Δx_{flow}, respectively).

DISCUSSION AND CONCLUSIONS

Our focus has been to delineate the fundamental features of Brownian motion that have a direct impact on single-molecule electrochemical detection. In real experiments, there are at least two additional factors that can significantly impact the quality of the information that can be extracted from amperometric data. The first is dynamic adsorption of analyte molecules to the electrode surface: intermittent adsorption results

in a decrease of the effective diffusion coefficient of the analyte in the detection region,[36] causing the current per molecule to have a value lower than the purely diffusive case $i_p = eD/z^2$. Furthermore, individual adsorption−desorption events add an additional component to the noise, although they are likely to occur on time scales much faster than the instrumental response and therefore likely to be averaged. Various approaches including the functionalization of electrodes with self-assembled monolayers with tailored end groups can be used to minimize adsorption.[37] A second aspect we have not considered so far is the background noise and contributions to it from instrumental noise, leakage currents, *etc.* Here we focused on an ideal scenario, where the only source of stochasticity is Brownian motion itself. Real experiments will have considerable extrinsic noise superimposed on the signal and thereby further obscure single-molecule features in the signals. As in most single-molecule techniques, elimination of the background noise is often as big a challenge as the selective amplification of the desired signal.

In summary, we have used random-walk simulations to elucidate the properties of redox-cycling-based nanogap sensors suitable for electrochemically detecting individual molecules. We argued that, while full 3D simulations can give insight into individual electron-transfer events, 1D random-walk simulations suffice to capture the dynamics that are experimentally accessible in channel-like nanogap detectors. These 1D simulations show that, in regimes where the detection region is diffusively coupled to a bulk reservoir, the inherently stochastic nature of Brownian motion coupled with the finite time resolution of measurement electronics causes significant deviations from the ideally expected Poisson distribution for the faradaic current. We have further explored three specific strategies by which this significant limitation can be overcome.

Our results show that the mechanical trapping of molecules in the detection region can ameliorate the smearing of the current distribution, as long as dead volumes can be neglected or that the signals are integrated for a sufficiently long time. Direct coupling of the detection volume to a 3D reservoir, on the other hand, leads only to minor enhancement of the quality of the signals. Finally, we showed that advective flow, wherein the solution containing the redox-active analyte is actively driven through the detection region, leads to essentially deterministic signals if the flow is sufficiently rapid. We propose that this latter approach offers the most promising route for overcoming stochasticity and creating reliable single-molecule detectors. The limitations imposed by the inherent nature of Brownian motion, as delineated in this paper, represent the key bottleneck in the wider adoption and utilization of single-molecule electrochemical sensitivity in more complex, realistic assays. However, the methods proposed herein to circumvent these hindrances can, in our view, enable a more widespread employment of this attractive capability.

METHODS

To compute the distribution of residence times of particles in the device, a single particle was injected at one end of the detection region (using $a = 20$) and the random-walk simulation was run until the particle exited either end of this region. The simulation was run repeatedly, and the total number of steps taken before exiting was histogrammed.

To simulate the behavior of molecules trapped in a closed volume, we considered the two edges of the 1D lattice ($a = 100$) to be perfectly reflecting boundaries. If a random walker took a step that would make it exit the simulated region, it was instead moved in the opposite direction.

To simulate the effect of coupling the ends of the detection volume to a 3D reservoir, we treated the detection region as a 1D lattice ($a = 100$) with perfectly absorbing boundaries. As particles undergoing the random walk touched the edges of the detection region, they were removed from the system. Simultaneously, new particles were introduced into the system at each time step and at each end of the detection region with a finite probability, p (where $p \ll 1$). Particles were thus introduced into the detection region at a rate $\Gamma_{in} = p/\Delta t$, while they exited with rate $\Gamma_{out} = \langle N \rangle/\tau_0$, where τ_0 is the mean lifetime of the particle in the detection region and $\langle N \rangle$ is the average number of particles in the detection region (or average occupancy); τ_0 can be evaluated numerically using $\tau_0 = (\Delta L^2/2D)\sum_n nP_{tot}(n)$. At steady state, $\Gamma_{in} = \Gamma_{out}$, so that $\langle N \rangle = p\tau_0/\Delta t$. The average number of particles present in the detection region is thus proportional to the parameter p; for our prototypical geometry, $p = 0.005$ corresponds to $\langle N \rangle = 1$.

To simulate the coupling of the detection region to a reservoir *via* a nanochannel, in which transport is also effectively 1D, we employed simulations on a large 1D lattice of 10^4 points. The detection region of the device was represented by a small subset of this large simulation domain ($a = 100$, or 1% of the total). The part of the simulation domain outside the detection region thus played the role of the nanochannel and was also sufficiently large to represent the reservoir. Periodic boundary conditions were enforced; particles exiting at one end of the simulation domain were reintroduced at the other end, ensuring that the "bulk" concentration remained constant throughout the simulation. The positions of a number of random walkers appropriate for the simulated concentration were randomly initialized; the walkers were moved independently at each time step, and the total number of molecules in the detection region was calculated after each step.

To simulate an advective flow of the solvent, a translation of magnitude $\Delta x_{flow} = v\Delta t$ was superimposed on the random-walk motion for each walker at each time step.

Conflict of Interest: The authors declare no competing financial interest.

Acknowledgment. We thank M. Zevenbergen, F. Pedaci, and S. Feldberg for insightful discussions. We gratefully acknowledge financial support from The Netherlands Organization for Scientific Research (NWO) and the European Research Council (ERC).

Supporting Information Available: Details of the full 3D random-walk simulation and the geometry used for particle confined in the detection region of a prototypical device. Histograms from simulated traces for particles trapped in the device with sealed boundaries and differing dead volumes. This material is available free of charge *via* the Internet at http://pubs.acs.org.

REFERENCES AND NOTES

1. Walter, N. G.; Huang, C.-Y.; Manzo, A. J.; Sobhy, M. A. Do-It-Yourself Guide: How To Use the Modern Single-Molecule Toolkit. *Nat. Methods* **2008**, *5*, 475–489.
2. Neuman, K. C.; Nagy, A. Single-Molecule Force Spectroscopy: Optical Tweezers, Magnetic Tweezers and Atomic Force Microscopy. *Nat. Methods* **2008**, *5*, 491–505.
3. Moerner, W.; Wild, U.; Basché, T. *Single-Molecule Optical Detection, Imaging and Spectroscopy*; John Wiley & Sons: New York, 2008.
4. Betzig, E.; Chichester, R. J. Single Molecules Observed by Near-Field Scanning Optical Microscopy. *Science* **1993**, *262*, 1422–1425.
5. Schmidt, T.; Schütz, G. J.; Baumgartner, W.; Gruber, H. J.; Schindler, H. Imaging of Single Molecule Diffusion. *Proc. Natl. Acad. Sci. U.S.A.* **1996**, *93*, 2926–2929.
6. Elf, J.; Li, G.-W.; Xie, X. S. Probing Transcription Factor Dynamics at the Single-Molecule Level in a Living Cell. *Science* **2007**, *316*, 1191–1194.
7. Yu, J.; Xiao, J.; Ren, X.; Lao, K.; Xie, X. S. Probing Gene Expression in Live Cells, One Protein Molecule at a Time. *Science* **2006**, *311*, 1600–1603.
8. Xie, X. S.; Yu, J.; Yang, W. Y. Living Cells as Test Tubes. *Science* **2006**, *312*, 228–230.
9. Anderson, L. B.; Reilley, C. N. Thin-Layer Electrochemistry: Use of Twin Working Electrodes for the Study of Chemical Kinetics. *J. Electroanal. Chem.* **1965**, *10*, 538–552.
10. Singh, P. S.; Goluch, E. D.; Heering, H. A.; Lemay, S. G. Nanoelectrochemistry: Fundamentals and Applications in Biology and Medicine. In *Applications of Electrochemistry and Nanotechnology in Biology and Medicine II*; Eliaz, N., Ed.; Springer: Berlin, 2012; Vol. 53, pp 1−66.
11. Fan, F. R. F.; Bard, A. J. Electrochemical Detection of Single Molecules. *Science* **1995**, *267*, 871–874.
12. Fan, F. R. F.; Kwak, J.; Bard, A. J. Single Molecule Electrochemistry. *J. Am. Chem. Soc.* **1996**, *118*, 9669–9675.
13. Bard, A. J.; Fan, F.-R. F. Electrochemical Detection of Single Molecules. *Acc. Chem. Res.* **1996**, *29*, 572–578.
14. Sun, P.; Mirkin, M. V. Electrochemistry of Individual Molecules in Zeptoliter Volumes. *J. Am. Chem. Soc.* **2008**, *130*, 8241–8250.
15. Zevenbergen, M. A. G.; Singh, P. S.; Goluch, E. D.; Wolfrum, B. L.; Lemay, S. G. Stochastic Sensing of Single Molecules in a Nanofluidic Electrochemical Device. *Nano Lett.* **2011**, *11*, 2881–2886.
16. Wolfe, R. L.; Balasubramanian, R.; Tracy, J. B.; Murray, R. W. Fully Ferrocenated Hexanethiolate Monolayer-Protected Gold Clusters. *Langmuir* **2007**, *23*, 2247–2254.
17. An alternative strategy relies on harnessing the electrocatalytic activity of nanoparticles toward either water oxidation or proton reduction reactions to amplify the electrochemical current, thereby enabling detection of single nanoparticles at inert substrate electrodes.[38]
18. Rassaei, L.; Singh, P. S.; Lemay, S. G. Lithography-Based Nanoelectrochemistry. *Anal. Chem.* **2011**, *83*, 3974–3980.
19. Kätelhön, E.; Wolfrum, B. On-Chip Redox Cycling Techniques for Electrochemical Detection. *Rev. Anal. Chem.* **2012**, *31*, 7–14.
20. White, R. J.; White, H. S. A Random Walk through Electron-Transfer Kinetics. *Anal. Chem.* **2005**, *77*, 214A–220A.
21. Nagy, G.; Sugimoto, Y.; Denuault, G. Three-Dimensional Random Walk Simulations of Diffusion Controlled Electrode Processes: (I) A Hemisphere, Disc and Growing Hemisphere. *J. Electroanal. Chem.* **1997**, *433*, 167–173.
22. Licht, S.; Cammarata, V.; Wrighton, M. S. Direct Measurements of the Physical Diffusion of Redox Active Species: Microelectrochemical Experiments and Their Simulation. *J. Phys. Chem.* **1990**, *94*, 6133–6140.
23. Licht, S.; Cammarata, V.; Wrighton, M. S. Time and Spatial Dependence of the Concentration of Less than 10^5 Microelectrode-Generated Molecules. *Science* **1989**, *243*, 1176–1178.
24. Zevenbergen, M. A. G.; Wolfrum, B.; Goluch, E. D.; Singh, P. S.; Lemay, S. G. Fast Electron-Transfer Kinetics Probed in Nanofluidic Channels. *J. Am. Chem. Soc.* **2009**, *131*, 11471–11477.
25. Kang, S.; Mathwig, K.; Lemay, S. G. Response Time of Nanofluidic Electrochemical Sensors. *Lab Chip* **2012**, *12*, 1262–1267.
26. Shen, M.; Arroyo-Currás, N.; Bard, A. J. Achieving Nanometer Scale Tip-to-Substrate Gaps with Micrometer-Size Ultramicroelectrodes in Scanning Electrochemical Microscopy. *Anal. Chem.* **2011**, *83*, 9082–9085.
27. Cutress, I. J.; Dickinson, E. J.; Compton, R. G. Electrochemical Random-Walk Theory: Probing Voltammetry with Small Numbers of Molecules: Stochastic *versus* Statistical (Fickian) Diffusion. *J. Electroanal. Chem.* **2011**, *655*, 1–8.
28. Amatore, C.; Grün, F.; Maisonhaute, E. Electrochemistry within a Limited Number of Molecules: Delineating the Fringe between Stochastic and Statistical Behavior. *Angew. Chem., Int. Ed.* **2003**, *42*, 4944–4947.
29. Nelson, P. *Biological Physics: Energy, Information, Life*; W.H. Freeman and Co.: New York, 2004; pp 117−118.
30. Redner, S. *A Guide to First-Passage Processes*; Cambridge University Press: Cambridge, UK, 2001; p 47.
31. Montroll, E. W. Random Walks on Lattices. III. Calculation of First-Passage Times with Application to Exciton Trapping on Photosynthetic Units. *J. Math. Phys.* **1969**, *10*, 753–765.
32. The Gambler's Ruin problem describes a betting game between two players with a unit amount and *a* units of money. At each step, one unit of money is gained or lost depending on the result of flipping an unbiased coin. The game ends when either of the two players has lost all their money.
33. Feller, W. *An Introduction to Probability Theory and Its Applications*, 3rd ed.; Wiley: New York, 1968; Vol. 1, p 353.
34. Schroeder, D. *An Introduction To Thermal Physics*; Addison-Wesley: New York, 2000; p 258.
35. Melin, J.; Quake, S. R. Microfluidic Large-Scale Integration: The Evolution of Design Rules for Biological Automation. *Annu. Rev. Biophys. Biomol. Struct.* **2007**, *36*, 213–231.
36. Zevenbergen, M. A. G.; Singh, P. S.; Goluch, E. D.; Wolfrum, B. L.; Lemay, S. G. Electrochemical Correlation Spectroscopy in Nanofluidic Cavities. *Anal. Chem.* **2009**, *81*, 8203–8212.
37. Singh, P. S.; Chan, H.-S. M.; Kang, S.; Lemay, S. G. Stochastic Amperometric Fluctuations as a Probe for Dynamic Adsorption in Nanofluidic Electrochemical Systems. *J. Am. Chem. Soc.* **2011**, *133*, 18289–18295.
38. Kwon, S. J.; Zhou, H.; Fan, F.-R. F.; Vorobyev, V.; Zhang, B.; Bard, A. J. Stochastic Electrochemistry with Electrocatalytic Nanoparticles at Inert Ultramicroelectrodes—Theory and Experiments. *Phys. Chem. Chem. Phys.* **2011**, *13*, 5394–5402.